A cryptotephra record from the Lake Victoria sediment core record of Holocene palaeoenvironmental change

Prof Christine S. Lane
Department of Geography, University of Cambridge, Downing Place, Cambridge, CB2 3EN, UK.
csl44@cam.ac.uk, +44 (0)1223 330242

Dr Catherine Martin-Jones
Department of Geography, University of Cambridge, Downing Place, Cambridge, CB2 3EN, UK.
cmm206@cam.ac.uk

Prof Thomas C. Johnson
Dept. of Geosciences, University of Massachusetts Amherst, Amherst, MA 01003, USA.
and
Large Lakes Observatory, University of Minnesota Duluth, 2205 E. 5th Street, Duluth, MN 55812, USA.
tcj@d.umn.edu

Abstract

The sediment record from Lake Victoria is an important archive of regional environmental and climatic conditions, reaching back more than 15,000 cal. years before present (15 ka BP). As the largest lake by area in East Africa, its evolution is key to understanding regional palaeohydrological change during the Late Pleistocene and Holocene, including controls on the Nile River flow. As well as important palaeoenvironmental proxies, the lake contains a unique record of explosive volcanism from the central Kenyan Rift, in the form of fine-grained volcanic ash (tephra) layers, interpreted as airfall deposits. In the V95-1P core, collected from the central northern basin of the lake, tephra layers vary in concentration from 10's to 10's of 1000's of glass shards per gram of sediment. None of the tephra are visible to the naked eye, and have only been revealed through careful laboratory processing. Compositional analyses of tephra glass shards has allowed the tephra layers to be correlated to previously unrecognized eruptions of Eburru volcano around 1.2 and 3.8 ka, and Olkaria volcano, prior to 15 ka. These volcanoes lie ~300 km east of the core site in the Kenyan Rift. Our results highlight the potential for developing cryptotephra analysis as a key tool in East African palaeolimnological research. Tephra layers offer opportunities for precise correlation of palaeoenvironmental sequences, as well as windows into the eruption frequency of regional volcanoes and the dispersal of volcanic ash.

Keywords

Tephra
Central Kenyan Rift
Volcanism
Holocene palaeoenvironment
Cryptotephra

1. Introduction

1.1. Lake Victoria

As Africa's largest lake by surface area, Lake Victoria plays a significant role in past and present hydrological processes of equatorial East Africa as well as much of north-eastern Africa via its contribution to local rainfall and to Nile River flow. The development of the lake through time is therefore of significant interest to palaeoclimatologists reconstructing past environmental changes, to biologists studying endemic and evolving species of plants, fish and other organisms, and to archaeologists interested in pathways of evolution, communication and migration for early to recent hominin species (e.g. Stager *et al*., 1997; Verheyen *et al*., 2003; Tryon *et al*., 2016).

Lake Victoria is believed to have been formed around 400,000 years before present (400 ka BP) as a result of tectonic uplift of the western arm of the East African Rift Valley, which reversed regional drainage and back ponding in its shallow basin (Johnson *et al*., 2000). Despite Lake Victoria's great age, our knowledge of the lake's palaeohydrological evolution is limited to the last ~18 ka BP. Since the 1960's, multiple sediment cores have been studied, most of which extend back to a significant desiccation event, marked by vertisol formation, coincident with the global Last Glacial maximum (LGM) (e.g. Kendall, 1969; Stager*et al*, 1984; Johnson *et al*., 1996; Talbot, and Lærdal, 2000). The onset, duration and continuity of Late Pleistocene desiccation is not known, as only undated seismic profiles are available to interpret the older part of the record (Scholz *et al*., 1998; Johnson *et al*., 2000). Shallow, unstable, lacustrine conditions, possibly interrupted by more than one interval of desiccation, existed prior to 15 ka BP, after which time the lake deepened and northerly overflow into the White Nile commenced (Beuning *et al*., 2002; Stager and Johnson*et al*, 2008). Over the last century, human impacts on Lake Victoria's ecosystem include eutrophication and consequent changes in aquatic resource availability (Verschuren *et al*., 2008).

Understanding how Lake Victoria's evolution relates to wider East African landscapes, as well as to regional and global climate variability, demands a precise and accurate chronology and a means to make direct and robust comparisons of the Lake Victoria record to neighbouring East African Rift archives, including lake sediment sequences and archaeological sites in Uganda, Rwanda, Kenya and Tanzania.

1.2 Tephrostratigraphy and cryptotephra in East Africa

The potential for using far-travelled volcanic ash (tephra) layers to date and correlate East African sedimentary records has been exemplified within Pleistocene archaeological research (e.g. Tryon and McBrearty, 2002, Brown and Fuller, 2008, Blegen *et al*., 2015). Undisturbed, airfall-derived, visible tephra layers provide isochrons that can be directly dated and geochemically fingerprinted, allowing outcrops to be correlated and ages transferred between sequences. The most widespread and well-characterized East African tephra layer of Late Pleistocene age to have been systematically characterized in such a way is the ~36 ka BP Menengai Tuff, found over an area of >115,000 km^2 (Blegen *et al*., 2016). The use of tephra to date and correlate lacustrine sediment core sequences has been more limited however, due to the paucity of visible tephra layers in some of the region's most important palaeoclimate archives.

A solution, which has been extensively applied across Europe and the North Atlantic region (e.g. Davies *et al*., 2010; Blockley *et al*., 2014), is to look for tephra layers that are not visible within their host sediments to the naked eye (termed *cryptotephra* by Lowe and Hunt (2001)). Cryptotephra investigations open up the possibility to trace airfall tephra layers over far wider distances from their source than visible tephra may be preserved. In doing so, the method increases the number of layers recorded in each sedimentary sequence and introduces the potential to connect archives within extensive regional (and possibly inter-continental) tephrostratigraphic frameworks (e.g. Lowe

et al., 2015; Lane *et al*., 2017). Whilst applications beyond the North Atlantic region are still relatively uncommon, the benefits of cryptotephra research are now being realized across eastern Africa. Far-travelled cryptotephra layers have shed light on debates around past climate and human evolution (Lane *et al.,* 2013) as well as providing unique dossiers of explosive volcanism (Martin-Jones *et al.,* 2017a,b) in eastern Africa.

This paper reports on a cryptotephra study from Lake Victoria, which aimed to identify non-visible tephra layers for the first time in this important regional Holocene palaeoenvironmental record. We demonstrate that cryptotephra layers can be located and identified to their source, then use our findings to illustrate the potential contribution that cryptotephra studies will make to palaeoclimate, volcanic hazards and archaeological research in eastern Africa.

2. Methods

2.1. Study site

Core V95-1P was collected from the northeastern part of Lake Victoria in 1995 (01°13.9′S, 33°11.9′E, 68 m water depth) (Fig. 1), as part of the International Decade of East African Lakes (IDEAL) research programme. The core samples the full Holocene lake sequence and continues back to the Late Pleistocene palaeosol(s). Multi-proxy sedimentary, palaeoenvironmental and palaeoclimatic analyses have documented the changing conditions of the lake, up to recent times (Johnson *et al*., 2000, Berke *et al*., 2012).

2.2 Cryptotephra investigations

To locate cryptotephra horizons, the full stratigraphy of the V95-1P core sediments was sampled at 10 cm contiguous and continuous intervals. Glass shards were extracted from the host sediments using the protocol described by Blockley *et al.* (2005). Dried and weighed sediment samples were sieved to >25 μm, and then the 1.95-2.55 g/cm^3 fraction from each sample was isolated using density separation with sodium polytungstate solution. The residues were mounted on glass slides in Canada Balsam and the number of glass shards from each sediment interval was counted using high-power transmitted light microscopy. Tephra glass shard concentrations were calculated as shard per gram of dry sediment (herein s/g) and the down-core shard counts plotted against the site's stratigraphy (Fig. 2). Intervals containing elevated tephra shard concentrations were then sampled at 1-2 cm resolution (depending on available material) and reprocessed to pinpoint more precisely the depth of each cryptotephra horizon. Shard distributions across a primary cryptotephra deposit in low-energy lacustrine sediments are typically characterized by a sudden peak in shard counts, which attenuates upwards through the stratigraphy (Davies *et al*., 2012). Isochron positions were identified at 1-2 cm resolution at the position of the shard peak and each tephra layer given a VT (Victoria Tephra) code based upon its core depth. Additional sediment was sampled from each tephra isochron to extract shards for geochemical characterization. Where shard concentrations suggested prolonged input of ash into the lake, preventing secure designation of an isochron position, multiple samples were selected to test whether the material derived from the same volcanic source.

Major and minor element concentrations of single glass shards in the Victoria tephra layers were determined using a JEOL 8600 wavelength dispersive electron microprobe analyser (WDS-EPMA) at the Research Laboratory for Archaeology and the History of Art (RLAHA, University of Oxford). The glass was analyzed using a defocussed 10 μm diameter beam operating at 15 kV and 6 nA. Sodium counts were collected over a 10 s acquisition, Cl and P for 60 s and all other analytes for 30 s. The instrument was calibrated against a suite of mineral and oxide standards, and a range of MPI-DING (Jochum *et al.,* 2005, 2006) glass compositions were analyzed as secondary standards to monitor instrument accuracy and as a means to quantify analytical precision. Due to the variable secondary hydration of glass, all compositional data presented in the text, tables and

graphs have been normalized to an anhydrous basis. See Supplementary Data file S1 for all raw data, secondary standards and analytical uncertainties.

To identify the volcanic source of a (crypto-) tephra layer, the composition of its glass shards must be matched to a comparable dataset from a securely dated and provenanced proximal eruption unit. Unfortunately, there are limited published data characterising Late Pleistocene to recent tephra erupted from Kenyan Rift volcanoes, and few eruptions have been precisely dated and described.
The works of MacDonald and Scaillet (2006), Marshall *et al*., (2009) and Clarke *et al*. (1990) provide a useful overview of central Kenyan Rift volcanism that stands as an important reference on composition and approximate timing of the largest eruptive events. Further whole rock compositional data exists from isolated petrological studies (e.g. Ren *et al*., 2006) and from tephra layers and obsidians from geologic sources and archaeological sites that pre-date the Lake Victoria sediment record (e.g. Brown *et al*., 2013; Tryon and McBrearty, 2002). Whilst there are challenges in the comparison of whole rock data, which may incorporate variable quantities of phenocrysts, with tephra glass analyses, as we generated for the Lake Victoria tephra layers, the central Kenyan Rift volcanoes have been shown to erupt distinct compositions (MacDonald and Scaillet, 2006). We therefore compared our results to all available datasets to identify the most likely sources of the Lake Victoria tephra layers.

2.3. Chronology

Previous age-models for the V95-1P sediment core (Johnson *et al*., 2000, Berke *et al*., 2012) were updated in this study using a Bayesian *P_Sequence* depositional model in OxCal version 4.3 (Ramsey, 2008, 2009) to allow robust interpolation between age estimates and full calculation of age-model uncertainties. The model uses all eight radiocarbon age measurements previously made on pollen and terrestrial macrofossils from the lacustrine diatomaceous sediments following Berke *et al*. (2012) and Johnson *et al*. (2000). Radiocarbon ages made on bulk sediment samples from the palaeosol intervals below 6 m core depth do not show a coherent increase of age with depth and are not included in the age model.
The *P_Sequence* model uses a variable k parameter for interpolation between dated horizons (Ramsey and Lee, 2013). In order to derive age-estimates for our cryptotephra layers, isochron positions were input using the Date_ function and model interpolated ages reported with 95% confidence intervals. Radiocarbon ages and full model parameters are detailed in Supplementary Data file S2.

3. Results:

3.1 Cryptotephra stratigraphy

Exploration of the V95-1P core sequence reveals six cryptotephra layers in varying shard concentrations within four discrete intervals of the sediment record (Fig. 2 and Table 1). The lower metre of the V95-1P core contained the highest concentrations of tephra glass shards and four samples were identified for analysis from this interval. Between ~600 and ~100 cm depth cryptotephra concentrations do not exceed 1 s/g, however shards reappear in uppermost metre and two further horizons were studied across this interval. Each cryptotephra-bearing interval is described here, beginning with the deepest (=oldest) layer and working upwards.

Cryptotephra layers VT683 & VT675: 690-670 cm depth
Tephra glass shards reach concentrations of >1000 s/g in the basal 20 cm of the sediments that were studied, with the exception of lower shard concentrations (663 s/g) (between 681-680 cm depth (Fig 2). The two samples with the highest concentrations across this 690-670 cm depth interval, identified here as VT683 (2800 s/g) and VT675 (3362 s/g) were prepared for compositional analyses to see if the tephra above and below the reduction in shard counts are

derived from the same volcanic episode. Both horizons contain clear shards of pumiceous, platy and bubble wall morphologies and ranging in size from ~50-150 µm (measured along the longest axis length).

Cryptotephra layers VT644 & VT636: 644-624 cm depth
A 50 cm interval from 644-624 cm depth contains the highest concentrations of glass shards seen throughout the Victoria archive (Fig 2). Two cryptotephra horizons are defined; VT644 at 644 -640 cm depth, with concentrations of >80,000 s/g, and another, VT636, with a peak of >60,000 s/g at 636 cm depth showing decreasing concentrations upward to 624 cm depth. Cryptotephra layers VT644 and VT636 contain transparent pumiceous, vesicular and bubble wall shards (Fig. 3). Glass shards in these horizons are the coarsest (50-400 µm) amongst the Victoria cryptotephras. These two high shard concentration layers are separated by four centimetres of sediment containing notably lower concentrations of glass, potentially suggesting on-going but variable deposition from a prolonged phase of volcanism.

Cryptotephra layer VT80: 84-78 cm depth
Cryptotephra VT80 occurs at 82-79 cm depth, and is the first appearance of shards following the ~600-100 cm interval of the Victoria sediments in which cryptotephra layers were not recorded (<1 s/g). The horizon contains extremely low shard concentrations of 40 s/g, represented by clear, platy, bubble-wall shards of <100 µm in size.

Cryptotephra layer VT22: 22-10 cm depth
The uppermost cryptotephra layer (VT22) is located at 22 cm depth, and contains ~12,000 s/g (Fig 2). The shards in VT22 vary in morphology from bubble wall, platy to pumiceous shards and vary in size from 50-100 µm.

3.2. Glass shard chemistry

The composition of glass shards in the six samples from the V95-1P cryptotephra horizons is summarized in Table 1 and Figure 4. Full compositional data are presented in Supplementary Data file S1. All cryptotephra layers are peralkaline rhyolites, defined by two distinct compositional populations. Excluding a single pantelleritic outlier, glass shards in the four oldest cryptotephra samples VT683, VT675; VT644 and VT636 contain 72.17-75.91 wt. % SiO_2, 9.67-11.07 wt. % Al_2O_3 and 3.11-3.70 wt.% FeO^T and can be classified as comendites. Glass shards in the two youngest cryptotephra layers VT80 and VT22 have pantelleritic compositions and contain lower SiO_2 (72.44-73.2 wt. %) and Al_2O_3 (8.17-8.45 wt. %) and higher FeO^T (6.18-6.68 wt. %) concentrations than older Victoria cryptotephras. The comenditic and pantelleritic tephra layers have eutectic glass compositions and cannot be clearly distinguished relative to other members of each group.

Due to their proximity in depth and indistinguishable major and minor element compositions, we are unable to prove with certainty whether the two lower pairs of cryptotephra layers, VT683 / VT675 and VT644 / VT636, each represent two eruptions within an extended period of volcanic activity, or intervals of reworking / delayed input of tephra within the lake-catchment system.

3.3 Modelled tephra ages

The updated Bayesian age-depth model for V95-1P shows approximately stable sedimentation rates (Fig. 5) throughout the 625 m diatomaceous mud unit, with age uncertainties at 95 % confidence intervals varying from 350-990 years in this upper part. No age model was run below 625 m, where radiocarbon dates from the sandy-palaeosol units show inconsistent age-depth

relationships. Consequently, only a minimum age estimate of >15,000 cal years BP can be made for the lower tephra layers: VT636, VT644, VT675 and VT683.

All tephra age-estimates are given in Table 2. Tephra layers VT80 and VT22 are dated to 3151-2537 cal yrs BP and 1973-1395 cal yrs BP respectively, representing two separate tephra depositional events that occurred in the late Holocene. A hiatus in tephra deposition lasted at least 12,000 years, prior to the eruption of VT80, suggestive of either an extended period of volcanic quiescence, reduced erupted ash volumes and/or changes in the atmospheric dispersal patterns of ash from eruptions in the nearby central Kenyan Rift.

4. Discussion

4.1 The volcanic sources of the Lake Victoria tephras

Figure 4 compares the glass composition of the Lake Victoria cryptotephra layers with published whole rock and obsidian data on samples from nearby central Kenyan Rift volcanoes. These comparisons should be made with caution, as whole rock analyses can contain variable quantities of phenocrysts, whilst glass (e.g. tephra shards and obsidian) analyses represent the magma composition at the time of the eruption. Aeolian fractionation processes may create compositional differences between samples from the same eruption by preferential removal of the densest (more basic) material and extended transport of the lightest (more evolved) material to the most distal localities. Typically, therefore, glass compositions appear more evolved than whole rock data and the latter may contain greater internal variability depending upon distance and direction of the sample from its eruptive source. Similarly, individual tephra samples and obsidians may show restricted compositions if they sample only part of an evolving magma composition from a particular phase of an eruption. Nonetheless, Kenyan Rift volcanoes erupt characteristically distinctive compositions in terms of their major elements (Fig. 4, MacDonald and Scaillet, 2006) and we exploit these geochemical signatures to test the potential sources of the Victoria cryptotephras here.

Five central Kenyan Rift volcanoes are known to have been active through the Quaternary-Recent. Menengai, Longonot and Suswa erupt trachytes and phonolites, whilst Eburru and Olkaria erupt trachytes and rhyolites (MacDonald and Scaillet, 2006; Fig. 4). Eburru and Olkaria are thus the only known Kenyan volcanoes to erupt peralkaline rhyolitic compositions

Glass shards in the Victoria tephra layers are comenditic to pantelleritic rhyolites - compositions erupted only from the Eburru and Olkaria volcanoes. The composition of glass shards in the four oldest Victoria tephra layers (VT683, VT675, VT644 and VT636) matches that of whole rock analyses from tuffs erupted from Olkaria and show a good affinity with Olkaria obsidian data (Marshall *et al.,* 2009; Brown *et al.,* 2013). A small compositional off-set between obsidian compositions related to Olkaria (Brown *et al*., 2013) and our distal tephra samples (Fig. 4), could be explained by analytical procedural differences, or compositional differences between different Olkaria eruptives, however it may merely represent sampling of material from a more distal location.

Previously published ages for eruptions of Olkaria are poorly constrained, being estimated only relative to closely-associated, dated, lava flows, tuffs and / or geomorphological features (MacDonald and Scaillet, 2009; Clarke *et al.* 1990). Four chronologically distinct volcanic episodes have previously been defined by Clark *et al*., 1990, occurring between 21 ka BP and the present. The oldest of these was an explosive phase dated to <21 ka and represented by the Olkaria Lower Comendite (OLC), found in outcrop close to Lake Naivasha. The OLC age is poorly constrained, being based on its stratigraphic relationship to tephra layers from Longonot, which are in turn dated relative to regional lake highstand events ~21 ka BP (Clarke *et al*., 1990). Three younger effusive

phases are dated to ~9 ka (the Olkaria Middle Comendite), ~6 ka (the Olkaria Lower Comendite) and ~180 a BP (the Ololbutot Comendite) (Clarke *et al.* 1990). Our discovery of far travelled tephra from Olkaria in Lake Victoria's sediments pre-dating 15 ka BP, most likely represents distal ashfall related to the earliest OLC explosive phase. Tentatively we therefore correlate VT636/VT644, which show the highest tephra shard concentrations in the Lake Victoria record, to this event. However, the record also appears to also capture an older, unknown Olkaria event in the lowermost tephra layers (VT675/VT683). There is growing evidence for earlier comenditic rhyolite eruptions of Olkaria, for example, Blegen *et al* (2015) describe a vitric ash, chemically correlated to Olkaria, pre-dating the 49 ka BP Nyamita tuff at the Kisaaka, Karungu locality, on the shores of modern Lake Victoria. Merrick *et al* (1994) also described obsidians of Olkaria composition, within Middle Stone Age archaeological sites and dating to >50 ka BP. It seems likely that a longer lake sediment core stratigraphy and further information from the proximal volcanic record would reveal a much extended eruptive history for Olkaria volcano.

Glass shards in the two youngest Victoria tephra layers (VT80 and VT22) bear an affinity to pantelleritic eruptives from Eburru, which contain lower SiO_2, Al_2O_3 and higher FeO^T concentrations than Olkaria whole rock and obsidian analyses (Fig. 4, Ren *et al.,* 2006; Brown *et al.,* 2013). The glass shards in VT22 and VT80 appear marginally more evolved than Eburru whole rock and obsidian compositions, showing ~1 % higher SiO_2 concentrations and ~1 wt. % less FeO^T than the most evolved proximal Eburru samples (Fig. 4). Once again, these differences are likely due to aeolian fractionation, reinforcing the concept that direct comparisons cannot always be made between different types of data and ideally proximal airfall ash from the same eruption would be available for direct comparison.

In summary, the V95-1P sediment core records prolonged or repeated comenditic eruptions from Olkaria occurring prior to 15 ka and two more recent, previously unrecorded pantelleritic eruptions from Eburru 3.8-1.2 ka. These cryptotephra layers are recorded >300 km from their respective source volcanoes (Fig. 1), illustrating that these eruptions were of sufficient magnitude to widely disperse fine-grained volcanic ash.

4.2 Toward a cryptotephra stratigraphy for eastern Africa

This is the first time that cryptotephra layers have been identified in the sediments of Lake Victoria, despite many decades of research on sediment cores from this iconic lake. Their correlation to Eburru and Olkaria volcanoes in the central Kenyan Rift, some 300 km away implies that these were voluminous eruption events and airfall-derived ash from these eruptions will most likely be identifiable as cryptic, or potentially visible layers, in other Late Pleistocene to Holocene lake sediment cores from the region. These horizons may in the future be established as isochrons that could provide precise tie-lines between palaeoclimate archives, facilitating robust comparison of environmental conditions over 100's of km distances in eastern Africa. It is interesting to note that the Olkaria tephra appear toward the top of the sandy-palaeosol units and thus predate the establishment of permanent lacustrine conditions (Fig. 2). Whilst in a subaerial environment tephra may be subject to weathering and reworking processes, the excellent tephra preservation and definition of the larger peaks in shard concentration indicate limited exposure. These layers in particular may provide potentially informative basin-wide as well as regional markers during a time of significant regional hydrological change.

4.3 Wider potential for multidisciplinary applications

The recent volcanic history for the Kenyan Rift remains poorly constrained (Siebert *et al.,* 2010) however the Lake Victoria tephra-record shows that both Eburru and Olkaria have erupted

explosively during the recent past. Our new cryptotephra correlations document and date Late Holocene explosive eruptions from Eburru for the first time. We also provide minimum ages that further constrain the timing of the last explosive eruption phase from Olkaria, represented in outcrop by the Olkaria Lower Comendites (Clark *et al*., 1990) and add to the growing evidence that Olkaria has been active for much longer than previously thought (e.g. Blegen *et al*., 2015). Further lake sediment tephra records could provide an effective means to document in detail the explosive eruptive history of central Kenyan volcanoes, as has been done for other regions of eastern Africa (Martin-Jones *et al.,* 2017a,b). Future explosive eruptions from the central Kenyan Rift volcanoes could present a threat to the population of Nairobi, located only ~80 km away, therefore robust eruption frequency information is important for our understanding of ash-fall hazards from little-studied volcanic centres.

Our Holocene record demonstrates that there is significant potential to develop a complete tephrostratigraphy for the Lake Victoria basin over longer time scales. Until now, much tephra research in eastern Africa has focused on the Pliocene to Middle Pleistocene palaeoanthropological sites (e.g. Feibel *et al*., 1999; Wolde-Gabriel *et al*., 2005; Tryon and McBrearty, 2006). Blegen *et al.* (2015) recently compiled a regional Late Pleistocene tephra framework for the Lake Victoria basin, and identified at least eight distinct eruptions across this interval, of which four produced widespread ash layers. This important work provides a first framework for the correlation and dating of anthropological sites during intervals crucial for modern human evolution and dispersal out of Africa. Extending this tephrostratigraphy to include palaeoenvironmental archives from regional lakes, such as from Lake Victoria, will tie human histories directly into nearby records of climate change.

5. Conclusions

Studying the rates and nature of past environmental changes is especially relevant in climatically sensitive regions such as eastern Africa, and underpinning these interpretations with high resolution chronology is paramount. In this paper we have highlighted the potential for using cryptotephra methodologies to build an event-stratigraphic framework for sediment sequences along the East African Rift. We have identified far-travelled ash-fall from two phases of explosive eruptive activity from Olkaria and Eburru volcanoes that may provide important markers for post LGM palaeoenvironmental and palaeohydrological evolution across the region.

Future work utilising similar approaches in nearby lake and archaeological sequences will extend the reach of a fledging regional tephrostratigraphy both in space and time. As tephra glass shard compositional datasets grow, challenges of correlating distal tephra layers will decrease. Studies of proximal outcrops, with complementary ash-fall glass analyses are needed to secure correlations of distal tephra to their volcanic source. This work therefore demands cooperation and data sharing between volcanologists, tephrochronologists and archaeologists, all of whom will benefit from a better understanding of the timing and impacts of explosive volcanism through the recent past.

6. Acknowledgements

The authors would like to recognize the contribution of Freiderike Murach-Ward for her assistance in processing laboratory samples, Dr. Nick Blegen for valuable discussions about central Kenyan tephra and Dr. Victoria Smith for support with EPMA. We also thank Anders Noren, Kristina Brady and the staff at LacCore, University of Minnesota, for their assistance accessing and sub-sampling the V95-1P sediment cores. Cryptotephra research was funded as part of a Leverhulme Trust Early Career Fellowship to CL.

Figures:

Fig. 1. Map showing the location of Lake Victoria in eastern Africa. The location of core V95-1P is indicated with a star. Volcanoes with suspected Holocene activity are marked by triangles (Eburru and Olkaria in orange), with those referred to in the text labelled.

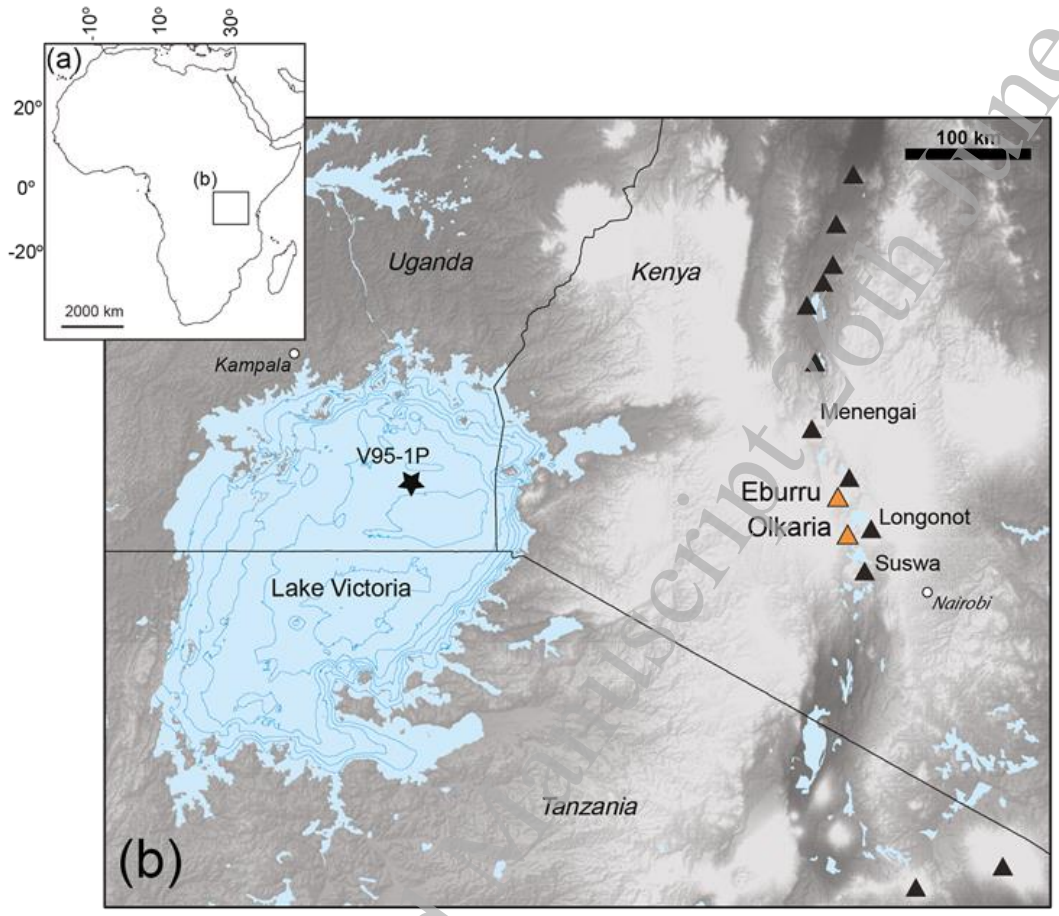

Fig. 2. Distribution of cryptotephra glass shards within the V95-1P sediment record. Left panel shows a whole core overview, alongside sediment core stratigraphy following Berke *et al*. (2012). Blow-outs A-D show shard distributions in detail for all tephra horizons, with shaded bars indicating the six samples analysed within this study.

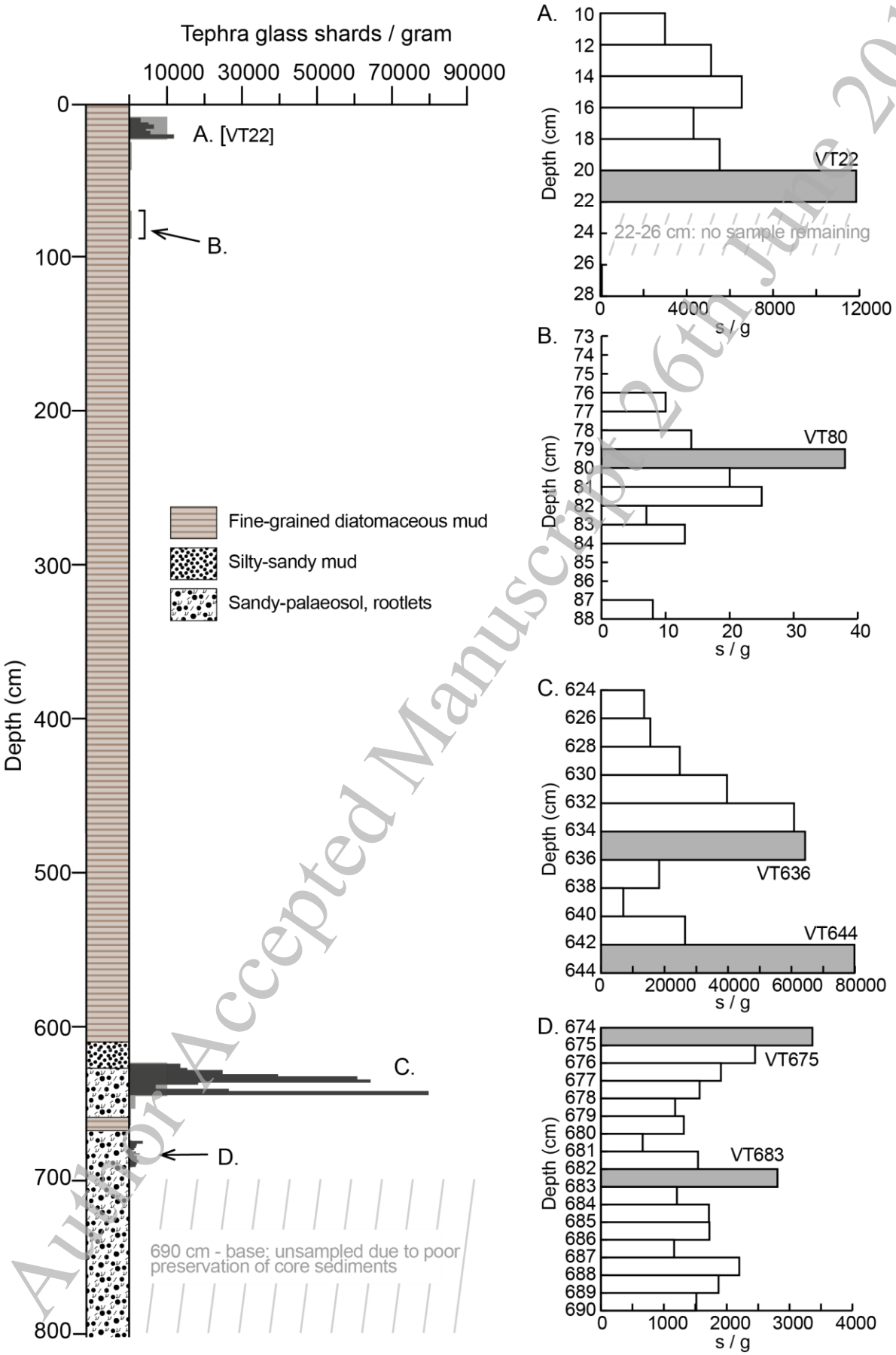

Fig. 3. Transmitted light photomicrographs of glass shards in the Lake Victoria cryptotephra layers (a) VT22, (b) VT675, (c) VT683, (d) VT636 and (e) VT644. (f) Outline drawings of selected glass shards illustrating typical pumiceous, vesicular, bubble wall and platy morphologies observed in the Lake Victoria cryptotephra layers. The cryptotephra layers contain transparent, pristine shards that range in size from 50-150 µm, however VT636 and VT644 contain grains of up to 400 µm.

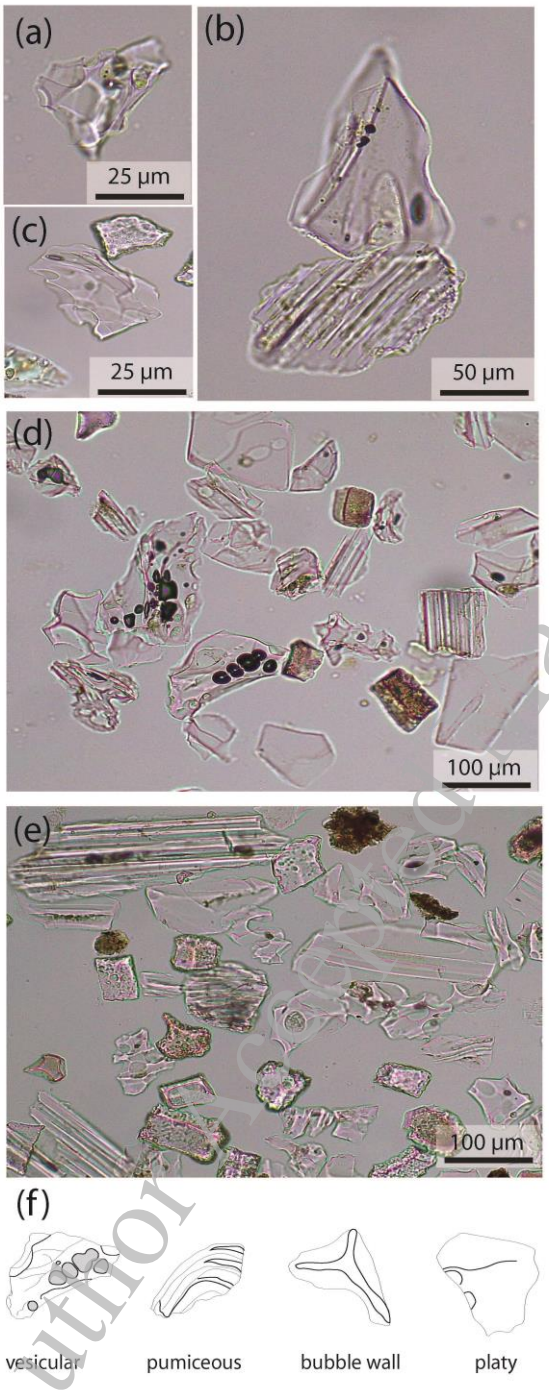

Fig. 4. Major element composition (wt. %) of single glass shards in the Lake Victoria cryptotephra layers, plotted alongside whole rock and obsidian glass analyses for the Olkaria and Eburru volcanoes (Ren *et al*., 2006; Marshall *et al*., 2009; Brown *et al*., 2013), with whole rock compositional envelopes for major volcanic centres in the Kenyan Rift adapted from MacDonald and Scaillet (2006). A) Total alkali silica diagram, showing that the Victoria cryptotephra glass shards are rhyolitic and their composition matches eruptives from Eburru and Olkaria, which are the only Kenyan Rift centres to erupt peralkaline rhyolites. B) and C) Bi-plots showing concentrations of FeO^T and SiO_2 versus Al_2O_3 in the Victoria cryptotephra shards. The four oldest cryptotephra layers (VT636, VT644, VT675 and VT683) are comenditic $Al_2O_3 > 1.33(FeO^T+4)$ (Le Maitre, 2002) and their glass composition correlates to published data on Olkaria. The two youngest horizons (VT22 and VT80) contain pantelleritic $Al_2O_3 < 1.33(FeO^T+4)$ glass shards which have similar compositions to eruptives from Eburru. All data normalized to water-free (100 wt. %) prior to plotting. Raw analytical data can be found in Supplementary Data file S1.

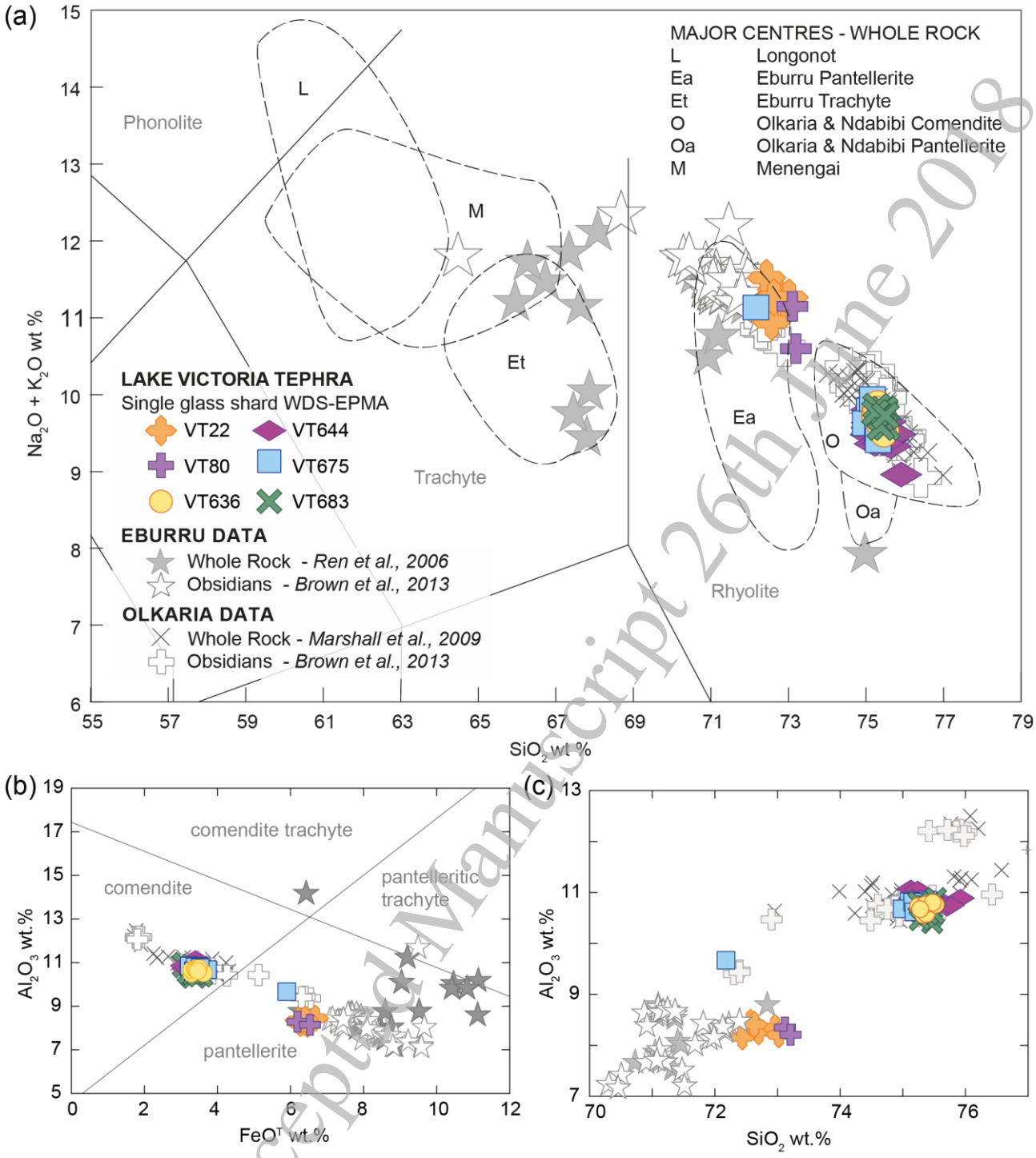

Fig. 5. Age-depth model for VP95-1P, showing constraints of cryptotephra ages (in blue). Bayesian *P*_Sequence deposition model for the upper lake sediment record (0--625 cm) run in OxCal version 4.3 (Ramsey *et al*., 2008, 2009). Probability distributions and interpolated age-depth model (in green) plotted with 95 % confidence intervals. Radiocarbon dates within the lower paleosol horizons (below 625 cm) are calibrated using IntCal13 (Reimer *et al*., 2013) but not included in the depositional model due to the significant scatter in measured ages. Full model parameters and references given in Methods and Supplementary Data file S2.

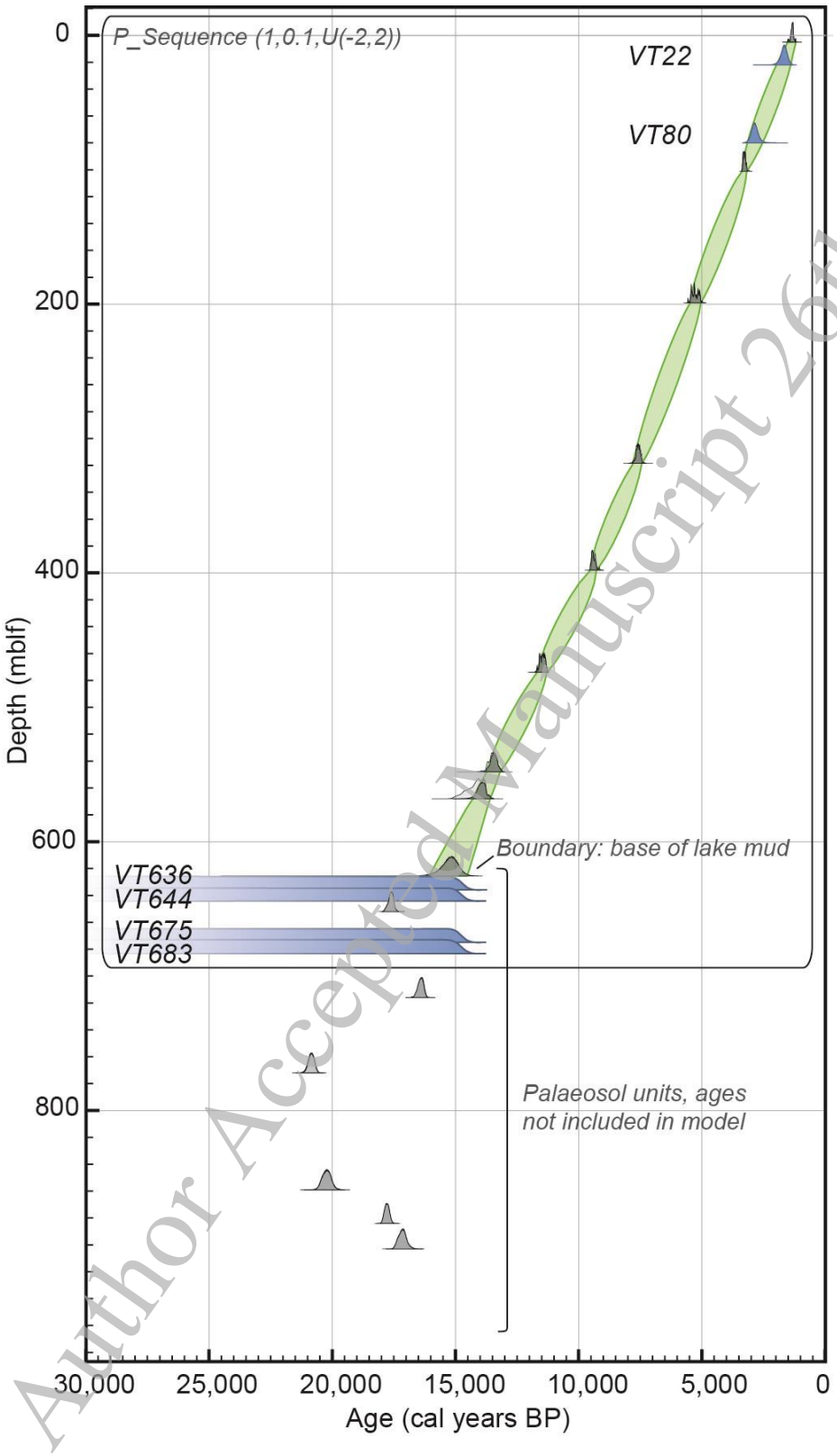

Tables:

Table 1. Averages and 2σ ranges for normalized major element composition (wt. %) of glass shards in each of the Lake Victoria cryptotephra layers. For the full geochemical dataset, see Supplementary Data file S1 (Table S2).

	VT22		VT80		VT636		VT642		VT675		VT683	
	average	*2 σ*	average	*2 σ*	average	*2 σ*	average	*2 σ*	average	*2 σ*	average	*2 σ*
	n=6		n=2		n=8		n=17		n=9		n=8	
SiO_2	72.72	*0.45*	73.16	*0.13*	75.35	*0.20*	75.41	*0.49*	74.89	*2.06*	75.41	*0.21*
TiO_2	0.21	*0.03*	0.22	*0.01*	0.17	*0.08*	0.16	*0.06*	0.18	*0.03*	0.19	*0.08*
Al_2O_3	8.31	*0.22*	8.27	*0.20*	10.69	*0.17*	10.84	*0.23*	10.63	*0.74*	10.62	*0.34*
FeO^T	6.39	*0.34*	6.35	*0.48*	3.42	*0.22*	3.32	*0.22*	3.68	*1.67*	3.34	*0.25*
MnO	0.19	*0.06*	0.18	*0.03*	0.04	*0.07*	0.05	*0.06*	0.06	*0.11*	0.05	*0.08*
MgO	0.01	*0.02*	0.00	*0.00*	0.00	*0.01*	0.01	*0.04*	0.01	*0.02*	0.01	*0.02*
CaO	0.25	*0.04*	0.20	*0.04*	0.16	*0.03*	0.15	*0.05*	0.20	*0.09*	0.17	*0.07*
Na_2O	7.03	*0.51*	6.84	*0.55*	5.27	*0.26*	5.09	*0.42*	5.34	*0.90*	5.28	*0.14*
K_2O	4.30	*0.17*	4.11	*0.23*	4.47	*0.15*	4.46	*0.18*	4.57	*0.15*	4.51	*0.16*
P_2O_5	0.02	*0.02*	0.01	*0.03*	0.01	*0.02*	0.01	*0.03*	0.01	*0.02*	0.01	*0.02*
Cl	0.57	*0.07*	0.68	*0.38*	0.43	*0.04*	0.49	*0.08*	0.43	*0.05*	0.42	*0.05*

Table 2. Summary of modelled ages (quoted with 95 % confidence intervals) and correlations for all six V95-1P cryptotephra samples.

Tephra sample	Core depth (cm)	Source volcano	Modelled age (yrs BP, 95.4% CL)
VT22	22	Eburru	1973-1395
VT80	80	Eburru	3151-2537
VT636	636	Olkaria	>15,000
VT644	644	Olkaria	>15,000
VT675	675	Olkaria	>15,000
VT683	683	Olkaria	>15,000

References

Berke, M. A., T. C. Johnson, J. P. Werne, K. Grice, S. Schouten, and J. S. S. Damsté. 2012. Molecular records of climate variability and vegetation response since the Late Pleistocene in the Lake Victoria basin, East Africa. Quaternary Science Reviews **55**:59-74.

Beuning, K. R., K. Kelts, J. Russell, and B. B. Wolfe. 2002. Reassessment of Lake Victoria–Upper Nile River paleohydrology from oxygen isotope records of lake-sediment cellulose. Geology **30**:559-562.

Blegen, N., C. A. Tryon, J. T. Faith, D. J. Peppe, E. J. Beverly, B. Li, and Z. Jacobs. 2015. Distal tephras of the eastern Lake Victoria basin, equatorial East Africa: correlations, chronology and a context for early modern humans. Quaternary Science Reviews **122**:89-111.

Blegen, N., F. H. Brown, B. R. Jicha, K. M. Binetti, J. T. Faith, J. V. Ferraro, P. N. Gathogo, J. L. Richardson, and C. A. Tryon. 2016. The Menengai Tuff: A 36 ka widespread tephra and its chronological relevance to Late Pleistocene human evolution in East Africa. Quaternary Science Reviews **152**:152-

168.

Blockley, S., S. Pyne-O'Donnell, J. Lowe, I. Matthews, A. Stone, A. Pollard, C. Turney, and E. Molyneux. 2005. A new and less destructive laboratory procedure for the physical separation of distal glass tephra shards from sediments. Quaternary Science Reviews **24**:1952-1960.

Blockley, S. P. E., A. J. Bourne, A. Brauer, S. M. Davies, M. Hardiman, P. R. Harding, C. S. Lane, A. MacLeod, I. P. Matthews, S. D. F. Pyne-O'Donnell, S. O. Rasmussen, S. Wulf, and G. Zanchetta. 2014. Tephrochronology and the extended intimate (integration of ice-core, marine and terrestrial records) event stratigraphy 8–128 ka b2k. Quaternary Science Reviews **106**:88-100.

Brown, F.H. and Fuller, C.R., 2008. Stratigraphy and tephra of the Kibish Formation, southwestern Ethiopia. Journal of Human Evolution, **55**:366-403.Brown, F., B. Nash, D. Fernandez, H. Merrick, and R. Thomas. 2013. Geochemical composition of source obsidians from Kenya. Journal of Archaeological Science **40**:3233-3251.

Clarke, M., D. Woodhall, D. Allen, and G. Darling. 1990. Geological, volcanological and hydrogeological controls on the occurrence of geothermal activity surrounding Lake Naivasha, Kenya. Republic of Kenya, Ministry of Energy.

Davies, S. M., P. M. Abbott, N. J. Pearce, S. Wastegård, and S. P. Blockley. 2012. Integrating the INTIMATE records using tephrochronology: rising to the challenge. Quaternary Science Reviews **36**:11-27.

Davies, S. M., S. Wastegård, P. Abbott, C. Barbante, M. Bigler, S. J. Johnsen, T. L. Rasmussen, J. P. Steffensen, and A. Svensson. 2010. Tracing volcanic events in the NGRIP ice-core and synchronising North Atlantic marine records during the last glacial period. Earth and Planetary Science Letters **294**:69-79.

Feibel, C. S. 1999. Tephrostratigraphy and geological context in paleoanthropology. Evolutionary Anthropology: Issues, News, and Reviews **8**:87-100.

Jochum, K. P., U. Nohl, K. Herwig, E. Lammel, B. Stoll, and A. W. Hofmann. 2005. GeoReM: a new geochemical database for reference materials and isotopic standards. Geostandards and Geoanalytical Research **29**:333-338.

Jochum, K. P., B. Stoll, K. Herwig, M. Willbold, A. W. Hofmann, M. Amini, S. Aarburg, W. Abouchami, E. Hellebrand, and B. Mocek. 2006. MPI-DING reference glasses for in situ microanalysis: New reference values for element concentrations and isotope ratios. Geochemistry, Geophysics, Geosystems **7**.

Johnson, T. C., K. Kelts, and E. Odada. 2000. The holocene history of Lake Victoria. AMBIO: A Journal of the Human Environment **29**:2-11.

Johnson, T. C., C. A. Scholz, M. R. Talbot, K. Kelts, R. Ricketts, G. Ngobi, K. Beuning, I. Ssemmanda, and J. McGill. 1996. Late Pleistocene desiccation of Lake Victoria and rapid evolution of cichlid fishes. Science **273**:1091-1093.

Kendall, R. L. 1969. An ecological history of the Lake Victoria basin. Ecological Monographs **39**:121-176.

Lane, C. S., B. T. Chorn, and T. C. Johnson. 2013. Ash from the Toba supereruption in Lake Malawi shows no volcanic winter in East Africa at 75 ka. Proceedings of the National Academy of Sciences **110**:8025-8029.

Lane, C. S., D. J. Lowe, S. Blockley, T. Suzuki, and V. Smith. 2017. Advancing tephrochronology as a global dating tool: Applications in volcanology, archaeology, and palaeoclimatic research. Elsevier.

Le Maitre, R., A. Streckeisen, B. Zanettin, M. Le Bas, B. Bonin, P. Bateman, G. Bellieni, A. Dudek, S. Efremova, and J. Keller. 2002. Igneous Rocks: A Classification and Glossary of Terms: A Classification and Glossary of Terms: Recommendations of the International Union of Geological Sciences, Subcommission on the Systematics of Igneous Rocks. Cambridge University Press UK.

Lowe, D. J., and J. B. Hunt. 2001. A summary of terminology used in tephra-related studies. Les Dossiers de l'Archaéo-Logis **1**.

Lowe, J. J., C. B. Ramsey, R. A. Housley, C. S. Lane, E. L. Tomlinson, R. Associates, and R. Team. 2015. The RESET project: constructing a European tephra lattice for refined synchronisation of environmental and archaeological events during the last c. 100 ka. Quaternary Science Reviews **118**:1-17.

Macdonald, R., and B. Scaillet. 2006. The central Kenya peralkaline province: insights into the evolution of peralkaline salic magmas. Lithos **91**:59-73.

Marshall, A., R. Macdonald, N. Rogers, J. Fitton, A. Tindle, K. Nejbert, and R. Hinton. 2009. Fractionation of peralkaline silicic magmas: The greater olkaria volcanic complex, Kenya Rift Valley. Journal of Petrology **50**:323-359.

Martin-Jones, C. M., C. S. Lane, N. Pearce, V. C. Smith, H. Lamb, C. Oppenheimer, A. Asrat, and F. Schaebitz. 2017. Glass compositions and tempo of post-17 ka eruptions from the Afar Triangle recorded in sediments from lakes Ashenge and Hayk, Ethiopia. Quaternary Geochronology **37**:15-31.

Martin-Jones, C. M., C. S. Lane, N. J. Pearce, V. C. Smith, H. F. Lamb, F. Schaebitz, F. Viehberg, M. C. Brown, U. Frank, and A. Asrat. 2017. Recurrent explosive eruptions from a high-risk Main Ethiopian Rift volcano throughout the Holocene. Geology **45**:1127-1130.

Merrick, H.V., Brown, F.H., Nash, W.P., 1994. Use and movement of obsidian in the Early and Middle Stone Ages of Kenya and northern Tanzania, in: Childs, S.T. (Ed.), Society, Culture, and Technology in Africa. MASCA, pp. 29-44.

Ramsey, C. B. 2008. Deposition models for chronological records. Quaternary Science Reviews **27**:42-60.

Ramsey, C. B. 2009. Bayesian analysis of radiocarbon dates. Radiocarbon **51**:337-360.

Ramsey, C. B., and S. Lee. 2013. Recent and planned developments of the program OxCal. Radiocarbon **55**:720-730.

Reimer, P. J., E. Bard, A. Bayliss, J. W. Beck, P. G. Blackwell, C. B. Ramsey, C. E. Buck, H. Cheng, R. L. Edwards, and M. Friedrich. 2013. IntCal13 and Marine13 radiocarbon age calibration curves 0–50,000 years cal BP. Radiocarbon **55**:1869-1887.

Ren, M., P. A. Omenda, E. Y. Anthony, J. C. White, R. Macdonald, and D. Bailey. 2006. Application of the QUILF thermobarometer to the peralkaline trachytes and pantellerites of the Eburru volcanic complex, East African Rift, Kenya. Lithos **91**:109-124.

Scholz, C., T. Johnson, P. Cattaneo, H. Malinga, and S. Shana. 1998. Initial results of 1995 IDEAL seismic reflection survey of Lake Victoria, Uganda and Tanzania. Pages 47-57 Environmental change and response in East African lakes. Springer.

Siebert, L., T. Simkin, and P. Kimberly. 2010. Volcanoes of the world, third edn. Smithsonian Institution. University of California Press, Berkeley, CA.

Stager, J. C. 1984. The diatom record of Lake Victoria (East Africa): the last 17, 000 years. *In* Proceedings of the seventh international diatom symposium: 455-476.

Stager, J.C., Cumming, B. and Meeker, L., 1997. A high-resolution 11,400-yr diatom record from Lake Victoria, East Africa. Quaternary Research **47:** 81-89.

Stager, J., and T. Johnson. 2008. The late Pleistocene desiccation of Lake Victoria and the origin of its endemic biota. Hydrobiologia **596**:5-16.Talbot, M. R., and T. Lærdal. 2000. The Late Pleistocene-Holocene palaeolimnology of Lake Victoria, East Africa, based upon elemental and isotopic analyses of sedimentary organic matter. Journal of Paleolimnology **23**:141-164.

Tryon, C. A., S. McBrearty, and P.-J. Texier. 2005. Levallois lithic technology from the Kapthurin formation, Kenya: Acheulian origin and Middle Stone Age diversity. African Archaeological Review **22**:199-229.

Tryon, C.A., Faith, J.T., Peppe, D.J., Beverly, E.J., Blegen, N., Blumenthal, S.A., Chritz, K.L., Driese, S.G., Patterson, D. and Sharp, W.D. 2016. The Pleistocene prehistory of the Lake Victoria

basin. Quaternary International, **404**: 100-114.

Verheyen, E., Salzburger, W., Snoeks, J. and Meyer, A. 2003. Origin of the superflock of cichlid fishes from Lake Victoria, East Africa. Science, **300** (5617): 325-329.

Verschuren, D., T. C. Johnson, H. J. Kling, D. N. Edgington, P. R. Leavitt, E. T. Brown, M. R. Talbot, and R. E. Hecky. 2002. History and timing of human impact on Lake Victoria, East Africa. Proceedings of the Royal Society of London B: Biological Sciences **269**:289-294.

WoldeGabriel, G., W. K. Hart, S. Katoh, Y. Beyene, and G. Suwa. 2005. Correlation of Plio–Pleistocene Tephra in Ethiopian and Kenyan rift basins: Temporal calibration of geological features and hominid fossil records. Journal of Volcanology and Geothermal Research **147**:81-108.

Supplementary Data file 1

Table S1 Major and minor element wt. % oxide compositions of individual tephra glass shards in each of the Lake Victoria V95-1P cryptotephra layers.

Tephra ID	Analysis date	SiO_2	TiO_2	Al_2O_3	MgO	FeO^T	MnO	CaO	Na_2O	K_2O	P_2O_5	Cl	Total
VT683	161013	69.16	0.22	9.53	0.02	3.07	0.03	0.15	4.86	4.16	0.01	0.43	91.64
VT683	161013	70.64	0.20	10.18	0.02	2.91	0.00	0.16	4.84	4.17	0.00	0.41	93.52
VT683	161013	69.48	0.20	9.70	0.00	3.06	0.02	0.11	4.82	4.27	0.00	0.39	92.07
VT683	161013	70.56	0.19	9.81	0.02	3.31	0.02	0.16	5.03	4.25	0.01	0.40	93.74
VT683	161013	69.96	0.15	9.81	0.00	3.09	0.09	0.22	4.96	4.10	0.00	0.39	92.78
VT683	161013	70.67	0.15	10.05	0.00	3.24	0.10	0.14	4.91	4.12	0.01	0.35	93.76
VT683	161013	70.45	0.13	10.12	0.00	3.12	0.08	0.15	5.01	4.20	0.00	0.36	93.61
VT683	161013	70.95	0.19	9.95	0.01	3.04	0.03	0.17	4.92	4.28	0.03	0.39	93.97
VT675	141013	70.20	0.16	10.11	0.00	3.19	0.07	0.14	4.97	4.25	0.03	0.37	93.49
VT675	141013	68.48	0.17	9.75	0.01	3.38	0.04	0.25	4.71	4.14	0.00	0.41	91.33
VT675	141013	69.89	0.17	10.05	0.02	2.97	0.04	0.15	4.68	4.27	0.02	0.43	92.71
VT675	141013	70.40	0.19	9.44	0.00	5.72	0.19	0.22	6.31	4.62	0.01	0.44	97.54
VT675	141013	71.62	0.15	10.29	0.00	3.28	0.07	0.14	4.82	4.34	0.01	0.40	95.12
VT675	141013	70.00	0.20	10.07	0.00	3.13	0.01	0.18	5.01	4.16	0.00	0.39	93.15
VT675	141013	68.97	0.16	9.74	0.02	3.04	0.01	0.22	4.99	4.20	0.02	0.39	91.76
VT675	141013	69.46	0.17	9.92	0.02	3.23	0.05	0.20	4.58	4.16	0.01	0.42	92.22
VT675	141013	71.22	0.15	10.02	0.00	3.13	0.05	0.17	4.99	4.31	0.02	0.40	94.46
VT644	300415	68.21	0.14	10.05	0.01	3.06	0.05	0.11	4.61	4.05	0.00	0.50	90.80
VT644	300415	69.12	0.18	9.81	0.00	2.92	0.08	0.15	4.55	4.11	0.05	0.55	91.52
VT644	300415	69.08	0.18	9.94	0.01	3.19	0.01	0.15	4.79	4.13	0.00	0.44	91.92
VT644	300415	70.17	0.13	10.07	0.01	2.97	0.03	0.15	4.13	4.22	0.05	0.52	92.43
VT644	300415	69.78	0.15	10.25	0.03	3.11	0.09	0.15	4.78	3.96	0.00	0.45	92.75
VT644	300415	69.98	0.18	10.09	0.01	3.03	0.05	0.15	4.74	4.17	0.00	0.44	92.83
VT644	300415	71.45	0.15	10.10	0.00	3.04	0.02	0.13	4.66	4.36	0.00	0.45	94.38
VT644	300415	71.29	0.15	10.30	0.00	3.06	0.06	0.16	4.90	4.20	0.01	0.44	94.57
VT644	300415	71.56	0.16	10.23	0.00	3.10	0.07	0.18	4.80	4.08	0.00	0.43	94.62
VT644	300415	71.58	0.15	10.22	0.00	3.11	0.06	0.14	4.73	4.25	0.00	0.46	94.71
VT644	300415	71.24	0.10	10.05	0.08	3.33	0.01	0.17	5.18	4.18	0.02	0.44	94.80
VT644	300415	71.87	0.10	10.20	0.00	3.06	0.04	0.12	4.77	4.29	0.00	0.43	94.88
VT644	300415	71.85	0.16	10.34	0.00	2.99	0.01	0.15	5.04	4.20	0.00	0.44	95.18
VT644	300415	71.93	0.13	10.38	0.00	3.24	0.03	0.18	4.78	4.21	0.00	0.48	95.37
VT644	300415	71.70	0.17	10.39	0.01	3.29	0.08	0.13	5.01	4.18	0.00	0.44	95.40
VT644	300415	71.71	0.18	10.36	0.00	3.29	0.10	0.11	5.01	4.19	0.00	0.45	95.42
VT644	300415	72.69	0.16	10.41	0.02	3.24	0.08	0.12	4.94	4.43	0.02	0.46	96.55
VT636	161013	68.94	0.21	9.65	0.00	3.00	0.06	0.13	4.92	4.18	0.01	0.42	91.52
VT636	161013	70.04	0.14	9.82	0.00	3.35	0.02	0.14	4.90	4.11	0.00	0.41	92.93
VT636	161013	69.91	0.18	9.95	0.01	3.05	0.07	0.16	5.06	4.09	0.02	0.41	92.91
VT636	161013	70.37	0.16	10.03	0.00	3.23	0.03	0.14	4.85	4.30	0.00	0.42	93.54
VT636	161013	71.02	0.16	10.11	0.00	3.17	0.00	0.14	4.87	4.14	0.02	0.41	94.04

VT636	161013	70.61	0.10	10.08	0.02	3.20	0.07	0.17	4.87	4.21	0.00	0.39	93.71
VT636	161013	71.15	0.12	10.18	0.00	3.28	0.00	0.14	4.81	4.19	0.02	0.41	94.28
VT636	161013	70.16	0.16	9.93	0.00	3.21	0.00	0.16	5.06	4.14	0.01	0.37	93.21
VT22	141013	70.37	0.22	8.01	0.00	6.12	0.15	0.26	6.83	4.25	0.01	0.59	96.80
VT22	141013	70.36	0.23	8.05	0.00	5.99	0.18	0.26	6.61	4.24	0.00	0.51	96.45
VT22	141013	70.74	0.18	7.95	0.00	6.07	0.14	0.21	6.88	4.11	0.01	0.56	96.87
VT22	141013	68.42	0.20	7.71	0.03	6.11	0.17	0.24	7.01	3.95	0.03	0.59	94.46
VT22	141013	70.57	0.19	8.22	0.01	6.49	0.23	0.26	6.49	4.23	0.01	0.54	97.24
VT22	141013	70.32	0.19	8.15	0.00	6.20	0.21	0.23	6.85	4.14	0.02	0.53	96.82
VT80	161013	70.96	0.21	8.09	0.00	6.00	0.17	0.21	6.82	4.07	0.02	0.52	97.06
VT80	300415	69.27	0.20	7.76	0.00	6.17	0.18	0.17	6.29	3.81	0.00	0.77	94.62

Table S2 Secondary standard analyses of MPI-DING fused volcanic glass standards, run intermittently during all Lake Victoria tephra glass shard EPMA runfiles to monitor instrument precision and accuracy. GeoRem assays for MPI-DING ATHO-G, StHs6/80-G and GOR-132 glass standards after Jochum *et al*. (2005, 2006).

MPI-DING standard	**Analysis date**	**SiO_2**	**TiO_2**	**Al_2O_3**	**MgO**	**FeO^T**	**MnO**	**CaO**	**Na_2O**	**K_2O**	**P_2O_5**	**Cl**	**Total**
ATHO-G	141013	75.23	0.26	12.17	0.09	3.20	0.15	1.79	2.97	2.74	0.02	0.09	98.70
ATHO-G	141013	75.02	0.25	12.32	0.09	3.15	0.09	1.74	3.96	2.72	0.02	0.03	99.39
ATHO-G	141013	74.99	0.28	12.35	0.07	3.15	0.16	1.80	4.13	2.65	0.04	0.06	99.69
ATHO-G	141013	75.46	0.23	12.29	0.12	3.50	0.15	1.62	4.14	2.79	0.01	0.05	100.36
ATHO-G	161013	74.89	0.24	12.21	0.12	3.31	0.19	1.75	4.04	2.68	0.03	0.03	99.49
ATHO-G	161013	74.55	0.25	11.86	0.10	3.39	0.04	1.73	4.34	2.71	0.03	0.04	99.03
ATHO-G	161013	74.53	0.27	12.01	0.10	3.14	0.13	1.73	4.04	2.78	0.02	0.05	98.80
ATHO-G	300415	75.04	0.25	12.01	0.05	3.17	0.07	1.73	3.96	2.77	0.04	0.04	99.14
ATHO-G	300415	74.75	0.23	12.09	0.05	2.95	0.10	1.70	4.07	2.65	0.02	0.08	98.70
ATHO-G	300415	74.11	0.25	12.06	0.11	2.96	0.05	1.74	4.17	2.70	0.00	0.04	98.18
ATHO-G	300415	74.72	0.25	12.06	0.10	3.07	0.09	1.72	4.29	2.69	0.00	0.03	99.03
ATHO-G	300415	74.60	0.25	11.91	0.06	3.05	0.12	1.66	4.12	2.76	0.00	0.03	98.56
ATHO-G	300415	75.34	0.25	12.49	0.07	3.38	0.07	1.61	4.33	2.69	0.00	0.07	100.30
ATHO-G	300415	75.74	0.26	12.20	0.07	3.23	0.17	1.66	4.22	2.68	0.03	0.04	100.30
	Average	**74.93**	**0.25**	**12.15**	**0.09**	**3.19**	**0.11**	**1.71**	**4.06**	**2.71**	**0.02**	**0.05**	
	2 σ	0.86	0.03	0.36	0.05	0.33	0.09	0.11	0.67	0.09	0.03	0.04	
	GeoReM	75.60	0.26	12.20	0.10	3.27	0.11	1.70	3.75	2.64	0.04	0.03	
MPI-DING standard	**Analysis date**	**SiO_2**	**TiO_2**	**Al_2O_3**	**MgO**	**FeO^T**	**MnO**	**CaO**	**Na_2O**	**K_2O**	**P_2O_5**	**Cl**	**Total**
StHs6/80-G	141013	62.90	0.69	17.60	2.04	4.35	0.00	5.28	4.53	1.32	0.18	0.00	98.88
StHs6/80-G	141013	63.62	0.77	17.81	1.99	4.46	0.14	5.27	4.71	1.27	0.16	0.02	100.23
StHs6/80-G	141013	63.54	0.69	17.74	1.92	4.04	0.03	5.29	4.80	1.34	0.14	0.02	99.54
StHs6/80-G	141013	63.05	0.75	17.52	1.93	4.18	0.11	5.16	4.61	1.27	0.14	0.02	98.74
StHs6/80-G	161013	63.40	0.77	17.52	1.94	4.39	0.08	5.16	4.66	1.30	0.17	0.00	99.39
StHs6/80-G	161013	63.43	0.74	17.61	2.01	4.22	0.04	5.22	4.53	1.35	0.14	0.00	99.28
StHs6/80-G	161013	63.21	0.70	17.49	1.99	4.13	0.00	5.24	4.36	1.31	0.16	0.02	98.62
StHs6/80-G	161013	63.28	0.71	17.37	1.93	4.34	0.08	5.02	4.55	1.26	0.15	0.00	98.69
StHs6/80-G	300415	63.61	0.74	17.75	1.98	4.38	0.06	5.18	4.55	1.26	0.13	0.01	99.65
StHs6/80-G	300415	63.84	0.74	17.69	2.06	4.34	0.12	5.24	4.53	1.29	0.22	0.03	100.10

StHs6/80-G	300415	63.81	0.71	17.69	1.98	4.40	0.04	5.26	4.51	1.25	0.15	0.02	99.82
StHs6/80-G	300415	63.69	0.75	17.54	1.96	4.18	0.05	5.27	4.58	1.26	0.10	0.02	99.39
StHs6/80-G	300415	63.45	0.71	17.47	1.92	4.20	0.04	5.24	4.29	1.33	0.12	0.00	98.78
StHs6/80-G	300415	63.38	0.74	17.57	1.88	4.41	0.10	5.19	4.43	1.35	0.16	0.02	99.23
StHs6/80-G	300415	63.21	0.75	17.42	1.89	4.37	0.10	5.25	4.50	1.32	0.17	0.01	98.98
	Average	**63.43**	**0.73**	**17.58**	**1.96**	**4.29**	**0.07**	**5.22**	**4.54**	**1.30**	**0.15**	**0.01**	
	2 σ	0.54	0.06	0.25	0.10	0.25	0.09	0.14	0.26	0.07	0.05	0.02	
	GeoReM	63.70	0.70	17.80	1.97	4.37	0.08	5.28	4.44	1.29	0.16	0.01	
MPI-DING standard	**Analysis date**	**SiO_2**	**TiO_2**	**Al_2O_3**	**MgO**	**FeO^T**	**MnO**	**CaO**	**Na_2O**	**K_2O**	**P_2O_5**	**Cl**	**Total**
GOR132-G	141013	45.59	0.31	10.84	22.16	9.94	0.10	8.46	0.80	0.04	0.03	0.01	98.28
GOR132-G	141013	45.69	0.27	10.93	22.23	9.95	0.11	8.26	0.84	0.04	0.07	0.00	98.40
GOR132-G	141013	45.47	0.28	10.91	21.89	9.91	0.11	8.40	0.80	0.04	0.03	0.00	97.82
GOR132-G	161013	45.37	0.34	10.63	22.22	9.84	0.14	8.54	0.92	0.02	0.04	0.00	98.06
GOR132-G	161013	45.66	0.31	10.62	22.39	10.41	0.27	8.51	0.79	0.03	0.05	0.00	99.03
GOR132-G	300415	44.86	0.25	10.77	22.46	10.40	0.08	8.56	0.75	0.07	0.07	0.01	98.27
GOR132-G	300415	44.78	0.27	10.75	22.48	10.11	0.15	8.61	1.02	0.04	0.03	0.00	98.25
GOR132-G	300415	44.73	0.32	10.54	22.26	10.12	0.11	8.59	0.80	0.00	0.06	0.02	97.56
GOR132-G	300415	45.08	0.30	10.68	22.58	10.58	0.11	8.57	0.74	0.00	0.04	0.02	98.68
GOR132-G	300415	45.24	0.23	10.83	22.23	10.36	0.15	8.62	0.78	0.03	0.03	0.00	98.49
GOR132-G	300415	45.20	0.28	10.66	22.24	10.17	0.17	8.43	0.84	0.01	0.04	0.02	98.06
	Average	**45.24**	**0.29**	**10.74**	**22.28**	**10.16**	**0.14**	**8.50**	**0.82**	**0.03**	**0.04**	**0.01**	
	2 σ	0.70	0.06	0.25	0.38	0.49	0.10	0.22	0.16	0.04	0.03	0.02	
	GeoReM	45.39	0.30	10.87	22.27	10.30	0.15	8.45	0.79	0.03	0.04	0.01	

Supplementary Data File 2

V95-1P Age Model Construction

Table S3: Radiocarbon dates for V95-1P, made on pollen, macrofossils and bulk sediment samples used in this study to construct a new Bayesian-based depositional model. References refer to the original publication for each age estimate. All dates were calibrated using IntCal13 (Reimer *et al*., 2013). Dates above a boundary placed at the onset of diatomaceous mud accumulation (610 m) were modelled using the P_Sequence function in OxCal version 4.3 (Ramsey *et al*., 2009, 2009). Age estimates within the palaeosol sediments are calibrated and excluded from the model due to the apparent age inconsistencies.

Depth (cm)	14C age (yrs BP)	±1sd	Material	Calibrated & modelled age (yrs BP, 95.4% CL)	Sample Code	Reference
5	1420	70	pollen	**1517-1182**	Trond 4/98	Johnson *et al*., 2000
101	3060	35	Sediment organic carbon	**3360-3178**	OS-77334	Berke *et al*., 2012
199	4595	75	pollen	**5475-5040**	Trond 4/98	Johnson *et al*., 2000
318.5	6700	110	pollen	**7786-7431**	Trond 4/98	Johnson *et al*., 2000
398	8380	70	pollen	**9531-9271**	Trond 4/98	Johnson *et al*., 2000
474	10000	40	Sediment organic carbon	**11694-11276**	OS-77335	Berke *et al*., 2012
548	11635	160	pollen	**13731-13188**	Trond 4/98	Johnson *et al*., 2000
568	12180	185	pollen	**14297-13583**	Trond 1/99	Johnson *et al*., 2000
Palaeosol levels:				**Calibrated age (yrs BP, 95.4% CL)**		
652	14450	65	Sediment organic carbon	**17,863-17,414**	OS-77351	Berke *et al*., 2012
716	13600	55	Plant / wood fragment	**16653-16,200**	OS-77314	Berke *et al*., 2012
772	17300	75	Bulk organic carbon	**21,089-20,603**	OS-77350	Berke *et al*., 2012
859	16760	140	*unspecified*	**20,585-19,870**	Beuning7/96	Berke *et al*., 2012
884	14600	60	Bulk organic carbon	**17,969-17,593**	OS-77336	Berke *et al*., 2012
903	14100	95	*unspecified*	**17,475-16,827**	Trond 1/99	Johnson *et al*., 2000

OxCal *P_Sequence* age model code:

```
Options()
{
 BCAD=FALSE;
};
Plot()
{
 P_Sequence("",1,0.1,U(-2,2))
 {
  Boundary()
  {
   z=800;
  };
  Date("T6")
  {
   z=683;
  };
  Date("T5")
  {
   z=675;
  };
  Date("T4")
  {
   z=644;
  };
  Date("T3")
  {
   z=636;
  };
  Boundary("DMudstart")
  {
   z=625;
  };
  R_Date("Trond 1/99",12180,185)
  {
   z=568;
  };
  R_Date("Trond 4/98-5",11635,160)
  {
   z=548;
  };
  R_Date("OS-77335",10000,40)
  {
   z=474;
  };
  R_Date("Trond4/98-4",8380,70)
  {
   z=398;
  };
  R_Date("Trond4/98-3",6700,110)
  {
   z=318.5;
  };
  R_Date("Trond4/98-2",4595,75)
  {
   z=199;
  };
  R_Date("OS-77334", 3060, 35)
  {
   z=101;
  };
  Date("T2")
  {
   z=80;
  };
  Date("T1")
  {
   z=22;
  };
  R_Date("Trond4/98-1",1420,70)
  {
   z=5;
  };
  Boundary();
 };
};
```